Soil Moisture Variability Intensifies and Prolongs Eastern Amazon Temperature and Carbon Cycle Response to El Niño–Southern Oscillation

PAUL A. LEVINE, JAMES T. RANDERSON, YANG CHEN, AND MICHAEL S. PRITCHARD

Department of Earth System Science, University of California, Irvine, Irvine, California

MIN XU AND FORREST M. HOFFMAN[a]

Climate Change Science Institute and Computational Earth Sciences Group, Oak Ridge National Laboratory, Oak Ridge, Tennessee

(Manuscript received 14 March 2018, in final form 19 November 2018)

ABSTRACT

El Niño–Southern Oscillation (ENSO) is an important driver of climate and carbon cycle variability in the Amazon. Sea surface temperature (SST) anomalies in the equatorial Pacific drive teleconnections with temperature directly through changes in atmospheric circulation. These circulation changes also impact precipitation and, consequently, soil moisture, enabling additional indirect effects on temperature through land–atmosphere coupling. To separate the direct influence of ENSO SST anomalies from the indirect effects of soil moisture, a mechanism-denial experiment was performed to decouple their variability in the Energy Exascale Earth System Model (E3SM) forced with observed SSTs from 1982 to 2016. Soil moisture variability was found to amplify and extend the effects of SST forcing on eastern Amazon temperature and carbon fluxes in E3SM. During the wet season, the direct, circulation-driven effect of ENSO SST anomalies dominated temperature and carbon cycle variability throughout the Amazon. During the following dry season, after ENSO SST anomalies had dissipated, soil moisture variability became the dominant driver in the east, explaining 67%–82% of the temperature difference between El Niño and La Niña years, and 85%–91% of the difference in carbon fluxes. These results highlight the need to consider the interdependence between temperature and hydrology when attributing the relative contributions of these factors to interannual variability in the terrestrial carbon cycle. Specifically, when offline models are forced with observations or reanalysis, the contribution of temperature may be overestimated when its own variability is modulated by hydrology via land–atmosphere coupling.

1. Introduction

El Niño–Southern Oscillation (ENSO) is the dominant mode of interannual climate variability in Earth's tropics. During the positive phase of the ENSO cycle (El Niño), high sea surface temperature (SST) anomalies in the eastern and central equatorial Pacific persist for several months during boreal fall and winter. Positive SST anomalies are associated with a weakened Walker circulation, which leads to climatic teleconnections globally, and particularly over the tropical land surface (Trenberth et al. 2002). Under El Niño conditions, the tropical land surface as a whole experiences anomalously high surface air temperatures, and anomalously low precipitation and terrestrial water storage, while the opposite occurs during the negative phase of the ENSO cycle (La Niña) (Llovel et al. 2011; Tyrrell et al. 2015; Reager et al. 2016).

ENSO-driven land surface responses are particularly prevalent in the Amazon River basin (Marengo 1992; Foley et al. 2002; Chen et al. 2011; de Linage et al. 2013). Recent El Niño events have exacerbated the effects of global warming, with the 2015/16 El Niño leading to

Denotes content that is immediately available upon publication as open access.

Supplemental information related to this paper is available at the Journals Online website: https://doi.org/10.1175/JCLI-D-18-0150.s1.

[a] Additional affiliation: Department of Civil and Environmental Engineering, University of Tennessee, Knoxville, Tennessee.

Corresponding author: Paul A. Levine, paul.levine@uci.edu

DOI: 10.1175/JCLI-D-18-0150.1

record-breaking temperatures and extreme drought in the Amazon (Jiménez-Muñoz et al. 2016). The Amazon is known as a ''hot spot'' of land–atmosphere coupling, in which variation in soil moisture leads to variation in the partitioning of turbulent surface fluxes between latent and sensible heat, subsequently influencing development of the planetary boundary layer and local atmospheric conditions (Fu et al. 2001; Lee et al. 2011; Ma et al. 2011; Sun and Wang 2013). An outstanding challenge is to determine how much the Amazonian temperature anomalies during different phases of the ENSO cycle are the direct result of atmospheric circulation changes due to SST variability, and how much they are indirectly driven by the local land surface response to moisture redistribution (Sun and Wang 2013; Spennemann and Saulo 2015; Levine et al. 2016).

The ENSO cycle is also associated with interannual variability in the atmospheric CO_2 growth rate (CGR), which increases during El Niño and decreases during La Niña (Bacastow 1976; Keeling and Revelle 1985; Jones et al. 2001). While interannual variability in the carbon sink of the tropical land surface has been strongly implicated in CGR variability, there is ongoing debate in the literature as to the exact mechanisms that lead to this relationship. Some studies attribute CGR variability primarily to the effects of temperature on terrestrial ecosystems (Cox et al. 2013; Piao et al. 2013; Wang et al. 2013, 2014). Other studies indicate that CGR is driven at least in part by the terrestrial response to precipitation and water storage variability (Foley et al. 2002; Zeng et al. 2005; Qian et al. 2008; Keppel-Aleks et al. 2014; J. Wang et al. 2016; Humphrey et al. 2018). While the relative importance of these drivers varies across tropical continents, both high temperature and low precipitation in the Amazon during a recent El Niño event were associated with an observed positive CO_2 flux anomaly (Liu et al. 2017).

Of course, the effects of temperature and hydrology on the terrestrial carbon cycle should not be viewed as mutually exclusive. The role of land–atmosphere coupling in the Amazon suggests that when considering the impact of SST forcing on terrestrial ecosystems, temperature anomalies and moisture redistribution may not be independent. However, studies exploring the relative importance of precipitation and temperature controls on terrestrial carbon cycle variability may obscure this interdependence by externally forcing land surface models with time series of these variables from observations or reanalysis (Zeng et al. 2005; Qian et al. 2008; Piao et al. 2013; Wang et al. 2013; J. Wang et al. 2016).

The Amazon's ecological response to ENSO is delayed by a series of cascading effects. ENSO teleconnections with the Amazon are strongest during boreal winter, with El Niño events decreasing precipitation between November and April (Chen et al. 2017). These months coincide with the dominant wet season for most of the Amazon. Therefore, even though years that begin under El Niño conditions may receive anomalously low precipitation during these months, the terrestrial ecosystem may not respond immediately, as water availability is not a limiting factor during the wet season. The Amazon rain forest is known to sustain plant growth during the dry season by utilizing water from deep soil, which can be hydraulically redistributed to the surface by deep roots (Nepstad et al. 1994; Lee et al. 2005) and transferred from groundwater into the root zone through capillary rise (Miguez-Macho and Fan 2012). Therefore, wet season precipitation deficits and concurrent radiation surpluses may reduce the soil moisture store for the subsequent dry season, leading to decreased evapotranspiration and primary production (Negrón Juárez et al. 2007; Chen et al. 2013; Hilker et al. 2014; Bowman et al. 2017; Liu et al. 2017; Swann and Koven 2017).

Here, we were motivated by the hypothesis that some portion of the Amazon temperature anomalies associated with ENSO was due to land–atmosphere coupling resulting from the cascading effects of precipitation and subsequent soil moisture anomalies. We posited that following El Niño events, drier soils in the Amazon would inhibit evaporative cooling, indirectly contributing to warmer temperatures above and beyond direct SST forcing. Furthermore, we hypothesized that the temperature

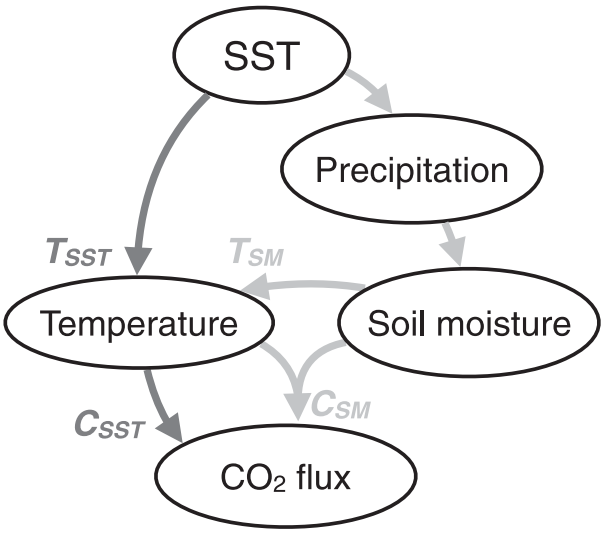

FIG. 1. Conceptual diagram of the hypothesized pathways through which SST and soil moisture variability impact temperature and the carbon cycle. T_{SST} is the portion of surface air temperature anomalies driven directly by remote SST forcing. T_{SM} is the portion of temperature anomalies driven indirectly by SST-driven soil moisture anomalies via land–atmosphere coupling. C_{SST} is the portion of the carbon cycle anomalies driven by T_{SST}. C_{SM} is the portion of the carbon cycle anomalies driven directly by soil moisture anomalies along with the portion of the temperature signal driven by soil moisture anomalies T_{SM}.

TABLE 1. Description of E3SM experiments and applicability to the conceptual pathways from Fig. 1.

Simulation	SST source	Soil moisture	Pathways
AMIP	Time-varying observations	Interactive from CLM4.5	All
SST_{var}	Time-varying observations	Prescribed from AMIP climatology	T_{SST} and C_{SST}
SM_{var}	Observations climatology	Prescribed from AMIP (time varying)	T_{SM} and C_{SM}
NO_{var}	Observations climatology	Prescribed from AMIP climatology	None

anomalies driven by land–atmosphere coupling may have contributed to variability in CO_2 fluxes between the terrestrial ecosystem and the atmosphere. This hypothesis is illustrated conceptually in Fig. 1.

To test this hypothesis, we performed a series of mechanism-denial experiments in an Earth system model. As described in section 2b, we first ran a control simulation driven by observed SSTs and with fully interactive land–atmosphere feedbacks. We then modified the land surface model to assimilate soil moisture in order to isolate the atmospherically mediated effects of remote SST variability on land surface temperature from those occurring indirectly as a result of SST-induced soil moisture anomalies. Our goal was to determine how much the cascading effects of SST anomalies on soil moisture anomalies contribute to interannual variability in surface air temperature and the net CO_2 flux over the Amazon basin.

2. Methods

a. Model description

We used version 0.3 of the Energy Exascale Earth System Model (E3SM), a branch of the Community Earth System Model (CESM), version 1.3 beta, that is now under development by the United States Department of Energy Office of Science (Terai et al. 2018). Global E3SM simulations were run in a configuration similar to the Atmospheric Model Intercomparison Project (AMIP) (Gates et al. 1999), with an interactive atmosphere and land surface, and with prescribed SSTs and sea ice fractions. The atmosphere was simulated by version 5.3 of the Community Atmosphere Model (Neale et al. 2012) with the spectral element dynamical core (CAM-SE) (Dennis et al. 2012), with the land surface simulated by version 4.5 of the Community Land Model with prognostic biogeochemistry (CLM4.5-BGC) (Oleson et al. 2013).

The prescribed SST and sea ice time series were from version 2 of the NOAA 1/4° daily Optimum Interpolation Sea Surface Temperature (OISSTv2) (Banzon et al. 2016). We chose this observationally based dataset in order to simulate the climatic response to the ENSO time series that took place during the observational record. Radiative forcing of greenhouse gas and aerosols was fixed at levels from the year 2000, so that the forced component of interannual variability would be due entirely to SST anomalies. We ran E3SM simulations on a cubed-sphere grid of NE30 (~100-km grid spacing), with 30 vertical layers in the atmosphere and 10 hydrologically active soil layers with exponentially increasing thicknesses to a depth of ~3.8 m. History fields were conservatively regridded to a 1° uniform equirectangular grid.

b. Experimental setup

The control run (hereafter referred to as the AMIP simulation) was forced with SSTs and sea ice fractions from daily OISSTv2 data from 1982 through 2016. Soil moisture was simulated interactively by CLM4.5-BGC, and recorded in each layer at every time step. We used this interannually varying time series of soil moisture from the AMIP simulation, as well as its climatology, to prescribe soil moisture in our subsequent experimental simulations (described below, and summarized in Table 1).

In the first experimental simulation (SST_{var}), we maintained interannual variability in the SST forcing, but we prescribed soil moisture in each layer to the annual climatology of the data from the AMIP simulation. This served to isolate the direct influence of SSTs on interannual variability in the Amazonian temperature T_{SST} (Fig. 1) and carbon cycle C_{SST}, while excluding the influence of soil moisture (T_{SM} and C_{SM}). Our approach was similar to the Global Land–Atmosphere Coupling Experiment of phase 5 of the Coupled Model Intercomparison Project (GLACE-CMIP5) (Seneviratne et al. 2013), but with prescribed SSTs that capture the observed ENSO time series.

In an additional experimental simulation (SM_{var}), we used a climatology of OISSTv2, but retained the interannual variability of soil moisture by prescribing the full time series of data from the AMIP simulation. This approach, which enabled us to isolate the indirect effects of SST-driven soil moisture variability from the direct effects of SST on atmospheric circulation, is similar to part of the experiment in Orth and Seneviratne (2017), but with a soil moisture time series that was created by forcing the climate model with observed SSTs. Finally, we performed a simulation that we refer to as NO_{var}, in which both SSTs and soil moisture were prescribed to a climatology. Comparing results from this simulation to the AMIP simulation enabled us to quantify the

unforced internal variability of the atmosphere apart from any contributions from either remote SST forcing or local soil moisture response.

c. Observations and reanalysis

The Amazon is a region where interannual variability of climate is known to be strongly related to interannual SST variability (Marengo 1992; Foley et al. 2002; Chen et al. 2011; de Linage et al. 2013). The AMIP simulation, driven by observed SSTs, was expected to reproduce the portion of the actual interannual variability of the Amazon climate that is controlled by SST-driven teleconnections, to the extent that the associated atmospheric bridge mechanisms are represented in the model. We benchmarked temperature, precipitation, and total water storage anomalies from the AMIP run with observational and reanalysis datasets in order to determine how well E3SM was able to reproduce ENSO teleconnections impacting the land surface.

For benchmark temperature data, we used version 4.01 of the Climatic Research Unit Time Series (CRU TS4.01; Harris et al. 2014), the European Centre for Medium-Range Forecasts interim reanalysis (ERA-Interim; Dee et al. 2011), and version 2 of the Modern-Era Retrospective Analysis for Research and Applications (MERRA-2; Gelaro et al. 2017). For benchmark precipitation data, we used version 2.3 of the Global Precipitation Climatology Project (GPCP v2.3; Huffman et al. 2009) and the CPC Merged Analysis of Precipitation (CMAP; Xie and Arkin 1997). Temperature and precipitation benchmark datasets were conservatively regridded to the same 1° equirectangular grid as the model. For total water storage benchmarks, we used version 2 of the Gravity Recovery and Climate Experiment (GRACE) Jet Propulsion Laboratory (JPL) RLO5M mascon solution (Watkins et al. 2015; Wiese et al. 2015). GRACE data were preserved in their original resolution of 3° mascons on a 0.5° grid, while modeled total water storage data were regridded to the same 0.5° grid and subsequently averaged over each of the 3° GRACE mascons.

d. Temporal classification and aggregation

We calculated a Niño-3.4 index that represented the mean SST anomaly averaged over the eastern tropical Pacific (5°S–5°N, 170°–120°W). The monthly OISSTv2 data were smoothed with a 3-month center-mean moving window, and the anomalies were estimated using a monthly climatology constructed from the entire time series (1982–2016). El Niño and La Niña years were defined as years that begin during an interval in which the Niño-3.4 index exceeds a threshold of +0.5°C and −0.5°C, respectively, for 5 or more consecutive months. According to these criteria, El Niño years in our analysis were 1983, 1987, 1988, 1992, 1995, 1998, 2003, 2005, 2007, 2010, 2015, and 2016, and La Niña years were 1985, 1989, 1996, 1999, 2000, 2001, 2008, 2011, and 2012.

To focus on interannual variability, we calculated monthly anomalies by subtracting linear trends and long-term means. Several of the analyses described below involved aggregating monthly anomalies into wet and dry seasons. We defined wet and dry seasons from a terrestrial perspective, based on the mean annual cycle of total water storage in the Amazon basin measured by GRACE. As such, the wet season comprised the 3 months with the largest increase in total water storage (January–March), whereas the dry season included the 3 months with the largest decrease (July–September).

The SST anomalies used to define El Niño and La Niña years generally exhibited their largest values (positive or negative) during or soon before the wet season. The initial onset of El Niño and La Niña conditions generally occurred around the end of the dry season. In consideration of the cascading response of the Amazon to ENSO (Chen et al. 2017), we associated the dry season that follows the peak of the SST anomaly with the El Niño or La Niña years. For example, the SST anomalies that defined the 1983 El Niño began at the end of the 1982 dry season, but we considered only the dry season in 1983 to be associated with this particular El Niño event.

e. Data analysis

1) Temperature variability decomposition

We assessed the relative contributions of various drivers of temperature variability by comparing the variance of temperature anomalies from the AMIP simulation with those from the experimental simulations. The magnitude of temperature variability resulting from remote SST forcing and local land–atmosphere coupling may not be additive, because feedbacks with the atmosphere are prevented in the simulations with prescribed soil moisture. However, subtracting the variance of temperature anomalies in the NO_{var} from those of SST_{var} and SM_{var} provides a useful indication of how much additional variability is due solely to the direct SST forcing and subsequent soil moisture response, respectively. Normalizing these quantities by the variance of the AMIP simulation indicates the relative importance of each of these mechanisms in explaining the overall variability of temperature.

2) Model benchmarking

To determine mean state biases, we compared wet- and dry-season multiyear means of temperature and accumulated precipitation in both the AMIP simulation and the benchmark data. We computed summary statistics (Taylor 2001) comparing monthly anomalies from benchmark datasets with those of the equivalent quantity in the AMIP

simulation to evaluate how well E3SM v0.3 was able to simulate observed interannual variability. To assess how realistically the model responds to ENSO, we compared correlations of the Niño-3.4 index with both model and benchmark data during the wet and dry season. Finally, to gauge whether the model exhibited the correct sensitivity of temperature to soil moisture, we replicated the analyses described below with the benchmark temperature datasets.

3) El Niño–La Niña contrast

We calculated mean anomalies of surface air temperature, terrestrial ecosystem fluxes, and relevant biogeophysical variables using all of the El Niño and La Niña years, respectively. The resulting mean El Niño and La Niña composites do not represent the temporal structure of individual years within the ENSO cycle. Nevertheless, they serve as useful indicators of the timing of the different drivers of variability across the experimental simulations.

We defined the ENSO-driven contrast as the difference between the mean El Niño and La Niña composites during the Amazonian wet and dry seasons. Calculating this metric for temperature and the net CO_2 flux provided the basis upon which we quantitatively estimated the conceptual pathways in our hypothesis (Fig. 1). We did not expect ENSO-driven contrasts to necessarily sum linearly between simulations, due to internal variability in addition to soil moisture feedbacks in the coupled AMIP simulation that were not captured by the mechanism-denial simulations. Therefore, we estimated each pathway as the range bounded on one side by the fraction of the contrast produced by including that mechanism, and on the other side by the fraction that denying that mechanism failed to produce. The width of the ranges provided an estimate of the importance of nonlinearities and soil moisture feedbacks (as well as any internal variability that may be present) in explaining the full contrast of the coupled AMIP simulation.

For example, to consider the conceptual pathways for temperature (T_{SST} and T_{SM} in Fig. 1), we first calculated the ENSO-driven contrast (EC) in temperature for the AMIP, SST_{var}, and SM_{var} simulations, notated as EC_{AMIP}, EC_{SST}, and EC_{SM} respectively, and then estimated each pathway as

$$T_{SST} \in \left\{ x \middle| \frac{EC_{SST}}{EC_{AMIP}} \le x \le \left(1 - \frac{EC_{SM}}{EC_{AMIP}}\right) \right\} \quad (1)$$

and

$$T_{SM} \in \left\{ x \middle| \frac{EC_{SM}}{EC_{AMIP}} \le x \le \left(1 - \frac{EC_{SST}}{EC_{AMIP}}\right) \right\}, \quad (2)$$

with an equivalent set of estimates for carbon fluxes (C_{SST} and C_{SM} in Fig. 1) based on the ENSO-driven contrast of NEE.

3. Results

a. Drivers of interannual variability in temperature

The overall variability in detrended monthly surface air temperature as simulated by E3SM had a variance of about 0.15°–0.45°C^2 throughout most of the Amazon (Fig. 2a), with a mean variance of 0.32°C^2 across the entire watershed. The fractions of the variance attributable to each driver were approximately additive, and indicated the relative importance of each driver across the watershed. The variability was relatively high in the south, as a consequence of contributions from internal atmospheric variability (Fig. 2b). In central and western portions of the basin, where the total variability was low, the variability was mostly driven by SST (Fig. 2c). The contribution from soil moisture variability was mainly observed in the eastern part of the Amazon basin (Fig. 2d).

b. Benchmarking E3SM with observations and reanalysis

1) Model validation

E3SM produced mean annual temperature within the range of the benchmark datasets over most of the Amazon, with the exception of the Andes. The AMIP run was warmer than the CRU TS4.01 data by approximately 2°–3°C, cooler than the ERA-Interim data by approximately 1°–2°C, and within about 1°C of the MERRA-2 data over the nonmontane portion of the basin (see Fig. S1 in the online supplemental material). The disagreement across benchmark data means that the bias between the model and any one dataset is less than the bias between the gridded observations from CRU and the reanalysis data. E3SM represented the magnitude of interannual variability within the range of the benchmark data (Fig. S2) and did a reasonable job simulating its timing (Fig. S3).

E3SM simulated a mean precipitation that was considerably lower than the observations from GPCP throughout most of the Amazon, producing excess rainfall only at the Andean margin (Fig. S4), with a bias pattern in this region consistent with other CMIP5 models (Joetzjer et al. 2013; Yin et al. 2013). A similar spatial pattern was evident in the magnitude of variability, as the ratio of modeled to observed standard deviations (of monthly anomalies) was low throughout most of the Amazon while high in the Andes (Fig. S5). Despite relatively low correlation of modeled precipitation anomalies with those of both precipitation datasets (Fig. S6), modeled terrestrial water storage anomalies during the dry season were correlated relatively highly with GRACE in the eastern Amazon

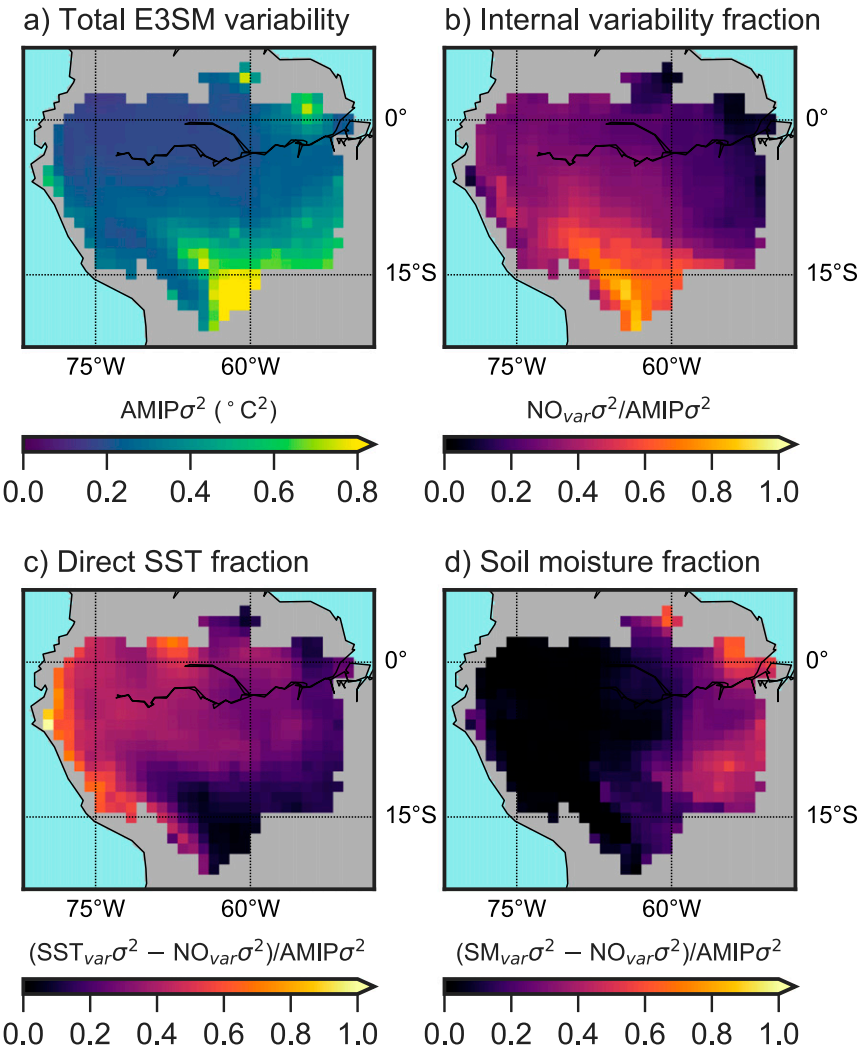

FIG. 2. Decomposition of interannual variability of surface air temperature in E3SM for 1982–2016. (a) Variance of detrended monthly temperature anomalies ($°C^2$) from the AMIP simulation. (b) Ratio of the variance of temperature anomalies from the NO_{var} simulation to that of the AMIP simulation. (c) Ratio of the difference between the variances of temperature anomalies from the SST_{var} and NO_{var} simulations to that of the AMIP simulation. (d) Ratio of the difference between the variances of temperature anomalies from the SM_{var} and NO_{var} simulations to that of the AMIP simulation.

(Fig. S7). This apparent contradiction likely results from the greater spatial homogeneity of water storage relative to precipitation; even if the model could not capture the precise spatial structure of precipitation anomalies, runoff distributed the resulting water storage anomalies more evenly.

2) BENCHMARKING THE ENSO–AMAZON TELECONNECTION

E3SM simulated reasonably well the relationship between Niño-3.4 SSTs during December–February and precipitation anomalies during subsequent wet (January–March) and dry (July–September) seasons (Fig. 3). SST anomalies were negatively correlated with wet-season precipitation in most of the northern Amazon basin, particularly toward the east, which was consistent with both benchmark datasets. Statistically significant positive correlations in the southern Amazon were present in E3SM but not in the benchmark data. During the dry season, E3SM showed a stronger negative correlation in the eastern Amazon than the GPCP precipitation data and, to a lesser extent, the CMAP data. However, the impact of this correlation bias only weakly affected soil moisture variability because of the smaller overall amount of precipitation during this time of year and carry-over in moisture storage from the previous wet season.

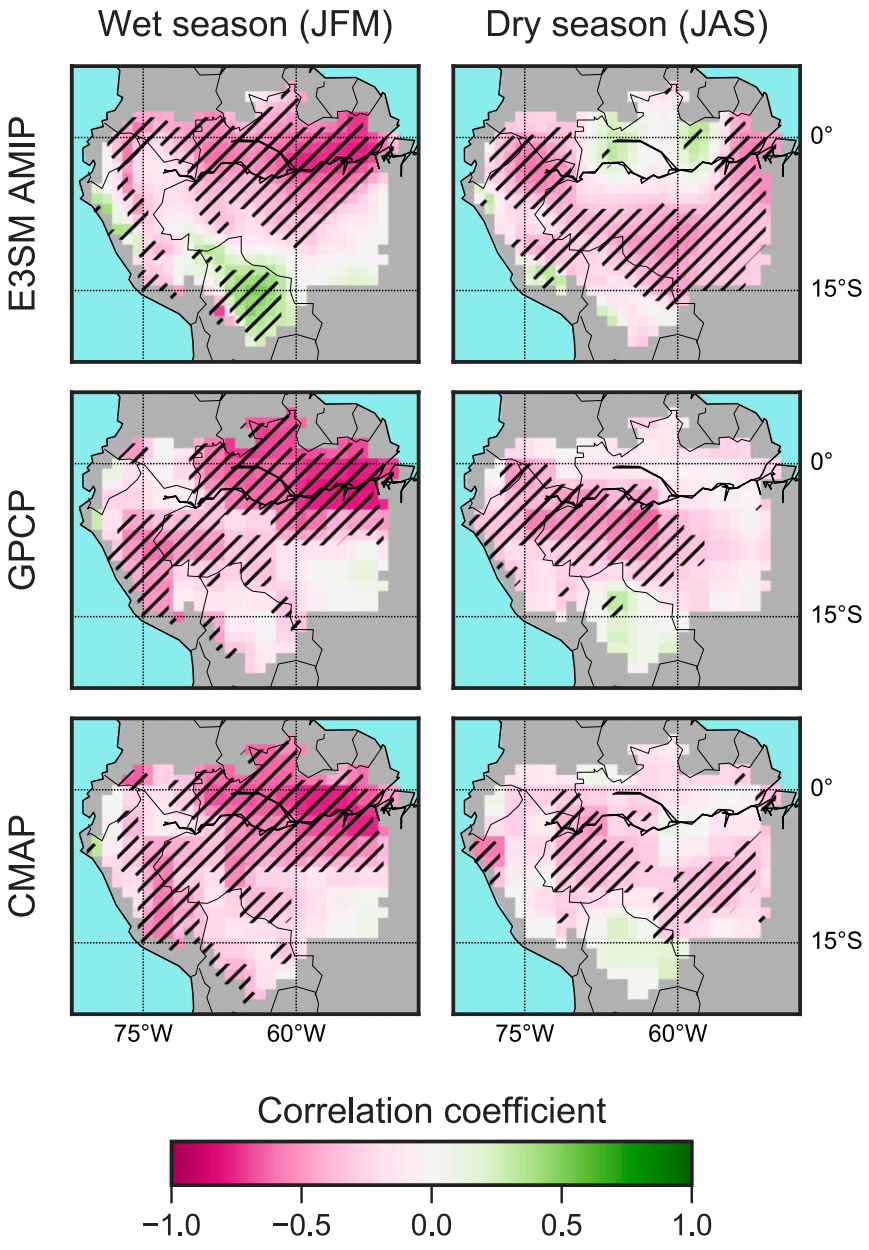

FIG. 3. Pearson's correlation coefficient comparing the Niño-3.4 index averaged over December–February with precipitation anomalies from (top) E3SM (AMIP simulation), (middle) GPCP v2.3, and (bottom) CMAP averaged over (left) the wet season (January–March) and (right) the dry season (July–September) for 1982–2016. Cross-hatching indicates the correlation coefficient was statistically significant at $p \leq 0.05$.

E3SM simulated ENSO teleconnections with total water storage in the Amazon qualitatively better than precipitation, compared with the available data from GRACE (Fig. 4). In the wet season, E3SM and GRACE showed a similar pattern, suggesting that evapotranspiration and runoff must have had compensating biases. In the dry season, there was less agreement between E3SM and GRACE in the west and central Amazon, but both the model and observations showed significant correlations in the east, despite less significant dry-season correlations in the benchmark precipitation data.

Although there were large differences among benchmark datasets, both model and benchmark data showed a positive correlation between the Niño-3.4 index and the surface air temperature anomalies in the Amazon during both the wet and dry seasons (Fig. 5). The correlations were higher in the wet season than in the dry season across all datasets. The dry season exhibited both the

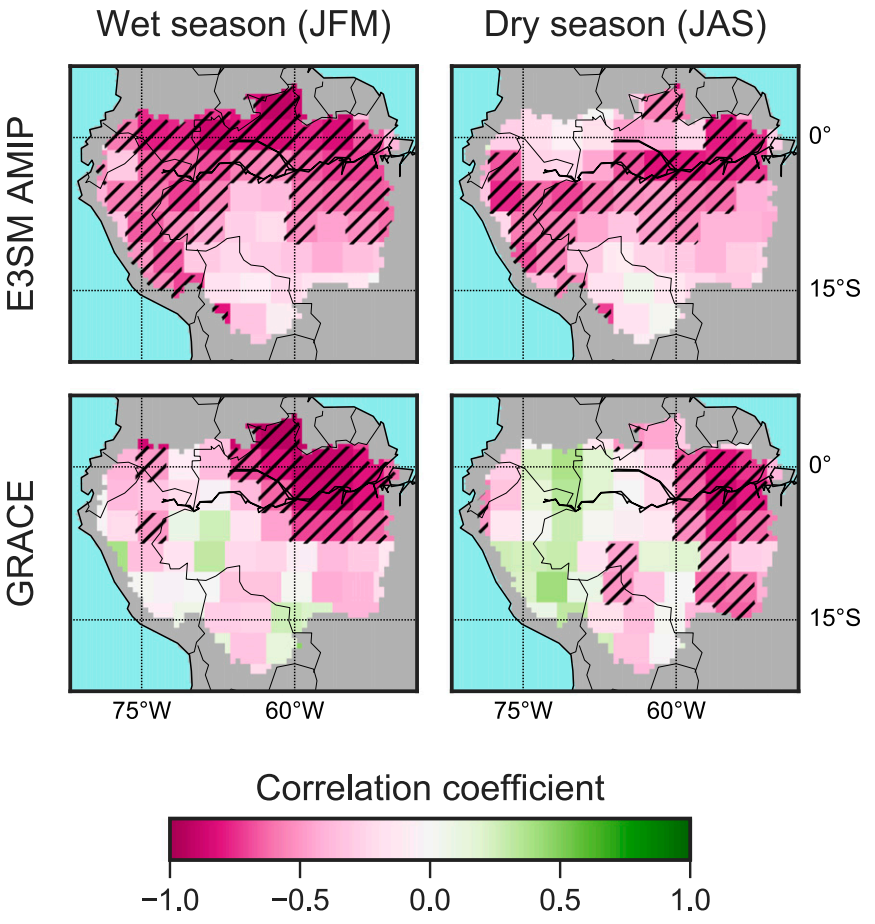

FIG. 4. Pearson's correlation coefficient comparing the Niño-3.4 index averaged over December–February with total water storage anomalies from (top) E3SM (AMIP simulation) and (bottom) GRACE averaged over (left) the wet season (January–March) and (right) the dry season (July–September) for 2003–16. Cross-hatching indicates the correlation coefficient was statistically significant at $p \leq 0.05$.

greatest disparity between benchmark datasets as well as the greatest disagreement between the model and benchmark data. E3SM and MERRAv2 both showed significant correlations across most of the Amazon during the dry season, but the ERA-Interim and CRU TS4.01 datasets each showed less.

c. *Amazon temperature response to ENSO forcing*

1) THE ENSO-DRIVEN CONTRAST

The ENSO-driven contrast in temperature from the different model experiments revealed the season when and location where temperature anomalies originated from direct SST forcing and land–atmosphere moisture coupling (Fig. 6). During the wet season, El Niño years exhibited higher temperatures than La Niña years throughout the Amazon, with most of the difference in the AMIP simulation attributable to forcing from remote SSTs (the SST_{var} simulation) and very little from land–atmosphere moisture coupling (the SM_{var} simulation). During the dry season, however, the ENSO-driven contrast was stronger in the SM_{var} simulation, particularly in the eastern part of the basin. Thus, land–atmosphere moisture coupling played a major role in determining the ENSO–temperature teleconnection during the dry season, and, more generally, in extending the duration of ENSO-induced temperature anomalies within the Amazon.

We further examined temperature anomalies in the eastern Amazon (east of 60°W) by exploring their temporal evolution during a full ENSO cycle (Fig. 7). Table 2 summarizes the seasonal means of wet- and dry-season contrasts in this region, which were used to quantitatively estimate our hypothesized conceptual pathways reported in Table 3. During the wet season in the eastern Amazon, the fully coupled (AMIP) temperature anomaly was 0.81°C higher for El Niño years than it was for La Niña years. Direct SST forcing

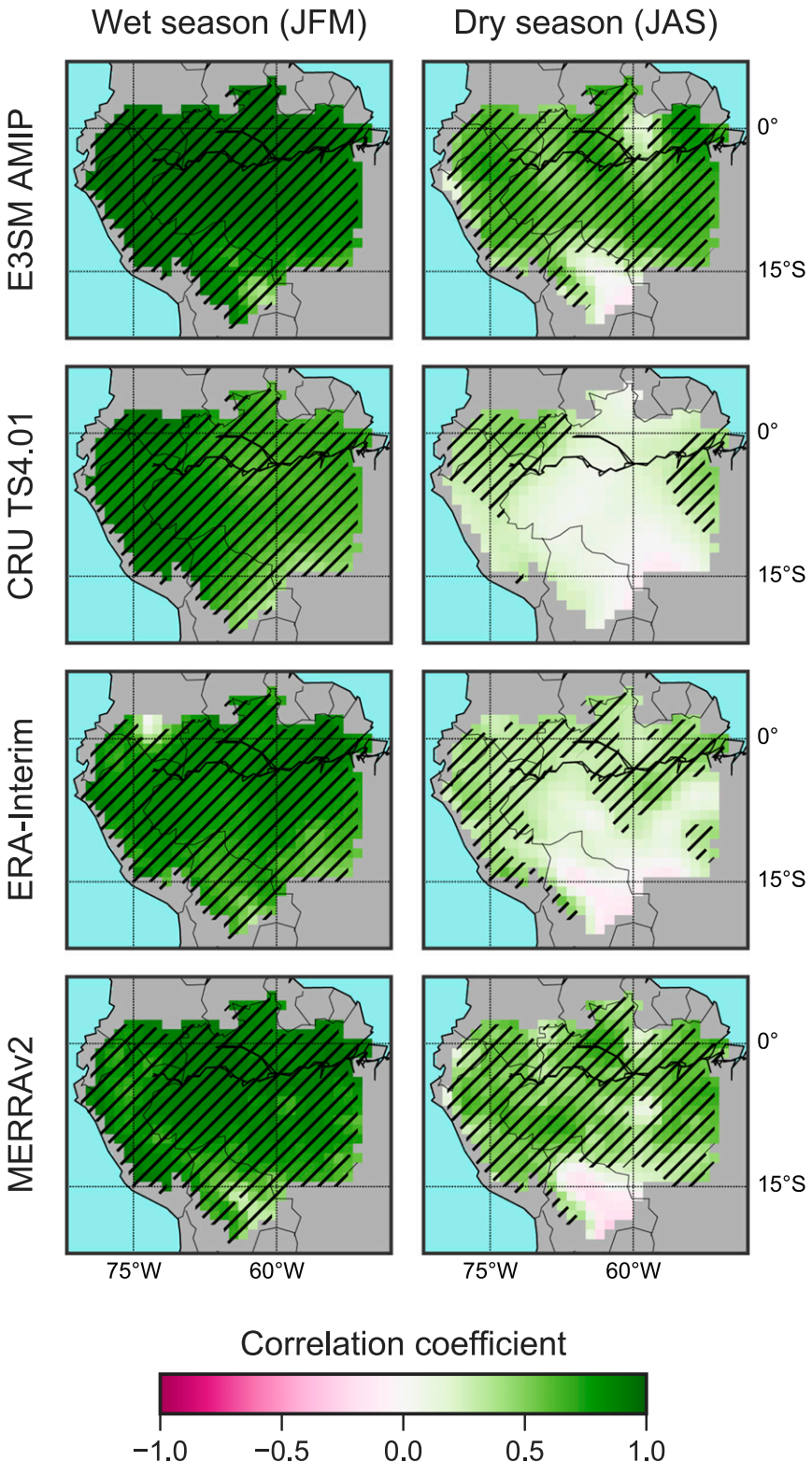

FIG. 5. Pearson's correlation coefficient comparing the Niño-3.4 index averaged over December–February with temperature anomalies from (top to bottom) E3SM (AMIP simulation), CRU TS4.01, ERA-Interim, and MERRA-2 averaged over (left) the wet season (January–March) and (right) the dry season (July–September) for 1982–2016. Cross-hatching indicates the correlation coefficient was statistically significant at $p \leq 0.05$.

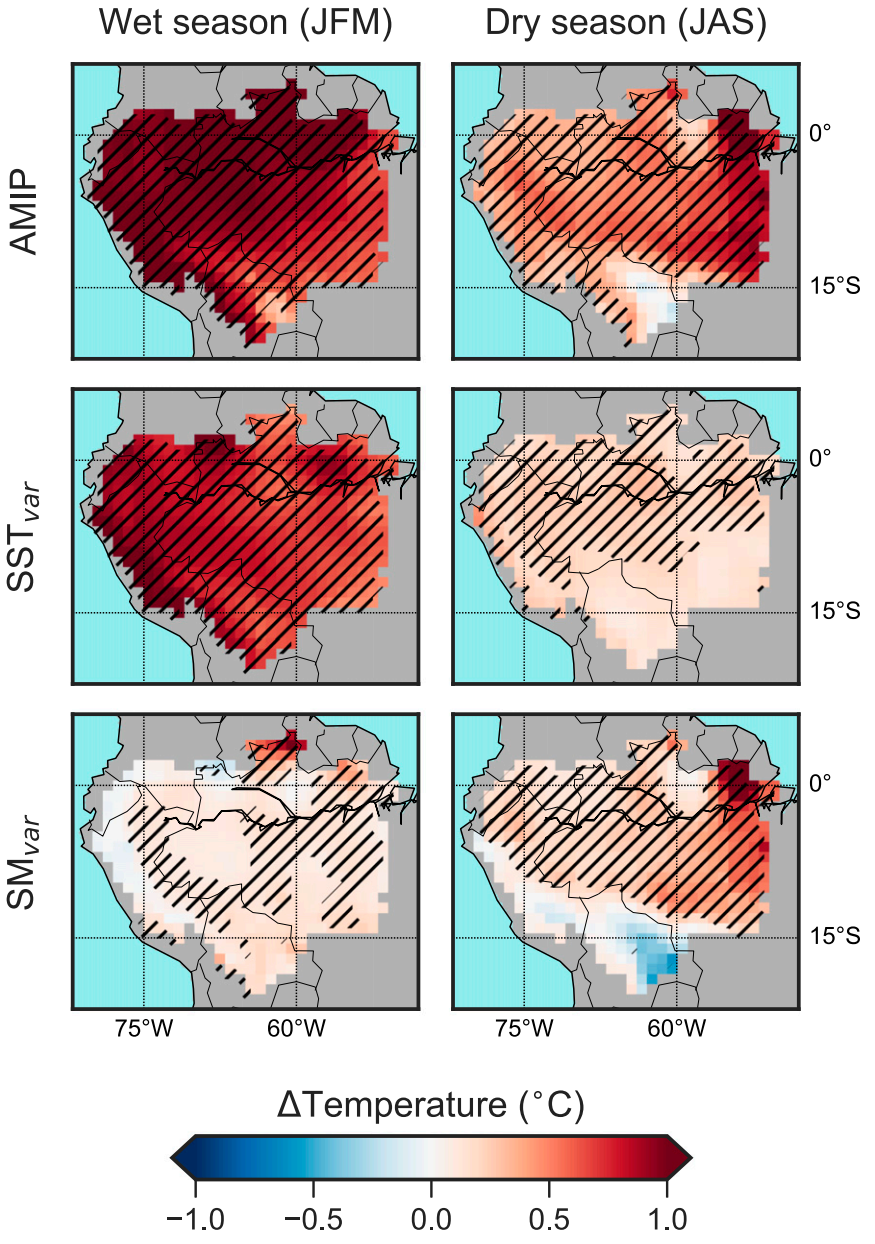

FIG. 6. Difference between surface air temperature anomalies averaged across El Niño and La Niña years during (left) the wet season (January–March) and (right) the dry season (July–September) in the (top) AMIP, (middle) SST_{var}, and (bottom) SM_{var} simulations. Cross-hatching indicates that the difference between El Niño and La Niña means is statistically significant at $p \leq 0.05$.

reproduced 81% of that anomaly when isolated in SST_{var}, and failed to reproduce 82% when denied in SM_{var}. Thus, wet-season T_{SST} was estimated as 81%–82%, and, similarly, T_{SM} as 18%–19%. During the dry season, the AMIP temperature anomaly showed a second peak of nearly the same magnitude (0.71°C). However, during this season, land–atmosphere moisture coupling was the dominant driver (T_{SM} = 67%–82%), while direct SST forcing had only a secondary effect (T_{SST} = 18%–33%).

2) DRIVERS OF THE ENSO TEMPERATURE CONTRAST

The role of land–atmosphere coupling in the eastern Amazon was evident in the time series of evapotranspiration, downwelling shortwave radiation (insolation),

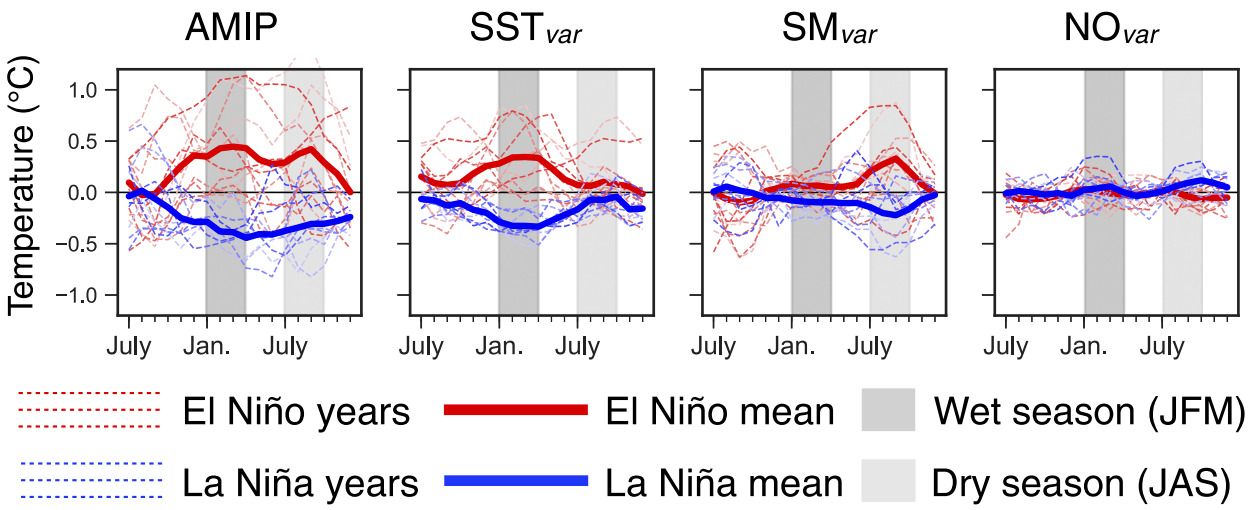

FIG. 7. Temporal evolution of monthly temperature anomalies in the eastern Amazon in the (left to right) AMIP, SST_{var}, SM_{var}, and NO_{var} E3SM simulations. Monthly surface air temperature anomalies were averaged across all grid cells in the Amazon watershed east of 60°W from the July preceding each El Niño (red) and La Niña (blue) year through the following December. Individual years are plotted with dashed lines, with a solid line for the mean of El Niño and La Niña years. Gray regions delineate the months in the wet season (January–March) and dry season (July–September). Monthly data were smoothed with a 3-month centered moving average for clarity.

and vapor pressure deficit (VPD) anomalies (Fig. 8). During the wet season, evapotranspiration and its drivers (insolation and VPD) from the AMIP simulation exhibited a positive relationship with the ENSO phase, consistent with an evaporative regime that is not moisture-limited (Seneviratne et al. 2010). This positive relationship was also present in the SST_{var} simulation (though somewhat weaker), and there was no wet-season evapotranspiration contrast in the SM_{var} simulation, indicating that evapotranspiration was limited by radiation, rather than moisture availability.

During the dry season, the AMIP simulation maintained a positive relationship between the ENSO phase and VPD, but the relationship with evapotranspiration was reversed, consistent with a moisture-limited evaporative regime. The similarly large contrasts in the SM_{var} simulation were consistent with the interpretation that soil moisture anomalies drove the temperature contrast during the dry season. Insolation contrasts were relatively low across the mean composites, but there was a large degree of noise in the individual years and high contrast in the NO_{var} simulation, indicative of higher internal variability during the dry season.

3) ENSO-DRIVEN TEMPERATURE CONTRAST IN BENCHMARK DATASETS

The E3SM temperature response to ENSO variability in the eastern Amazon falls within the range of available benchmark datasets (Fig. 9). Both the ERA-Interim and, in particular, the CRU TS4.01 datasets showed a much weaker contrast throughout the year, and particularly during the dry season, than the E3SM AMIP simulation. However, MERRA-2 showed a somewhat stronger temperature contrast than the E3SM AMIP simulation, and it is the only benchmark dataset that, like E3SM, showed a dry-season contrast as strong as the

TABLE 2. Differences between mean El Niño and mean La Niña anomalies in eastern Amazon (east of 60°W). The net ecosystem exchange is a positive flux to the atmosphere. It is the balance between net primary production (positive is flux to the land surface) and heterotrophic respiration (positive is flux to atmosphere), though the rows may not sum perfectly due to rounding error.

	Wet season (JFM)			Dry season (JAS)		
	AMIP	SST_{var}	SM_{var}	AMIP	SST_{var}	SM_{var}
Temperature (°C)	0.81	0.67	0.15	0.71	0.13	0.48
Vapor pressure deficit (hPa)	55.1	24.2	23.0	204	31.9	162
Insolation (W m^{-2})	7.69	2.04	4.34	1.83	2.13	−0.65
Evapotranspiration (mm day^{-1})	0.12	0.08	0.03	−0.27	0.01	−0.31
Net primary production (gC m^{-2} day^{-1})	−0.16	−0.07	−0.07	−0.47	−0.02	−0.43
Heterotrophic respiration (gC m^{-2} day^{-1})	−0.01	0.07	−0.08	−0.16	0.00	−0.17
Net ecosystem exchange (gC m^{-2} day^{-1})	0.16	0.14	−0.01	0.32	0.03	0.27

TABLE 3. Contribution of SST and soil moisture variability to the differences in temperature and the net CO_2 flux (see Fig. 1) between mean El Niño and mean La Niña anomalies, as percentage of the difference in the AMIP simulation, in eastern Amazon (east of 60°W).

	Temperature		Net ecosystem exchange	
	T_{SST}	T_{SM}	C_{SST}	C_{SM}
Wet season	81%–82%	18%–19%	89%–108%	−8%–11%
Dry season	18%–33%	67%–82%	9%–15%	85%–91%

one from the wet season. The disagreement between benchmark datasets presented a challenge to evaluating the model; however, there was some indication that the temperature response to ENSO in E3SM may be too strong, particularly in response to soil moisture variability during the dry season.

4) LAG-CORRELATION ANALYSIS

A lag-correlation analysis demonstrated how soil moisture variability in E3SM served to intensify and prolong the response of temperature in the eastern Amazon to SST forcing from the Niño-3.4 region (Fig. 10a). The SST_{var} simulation exhibited the maximum correlation between SST anomalies and eastern Amazon surface air temperature anomalies with a 2- or 3-month lag in air temperature. The SM_{var} simulation exhibited a weaker but still significant maximum correlation

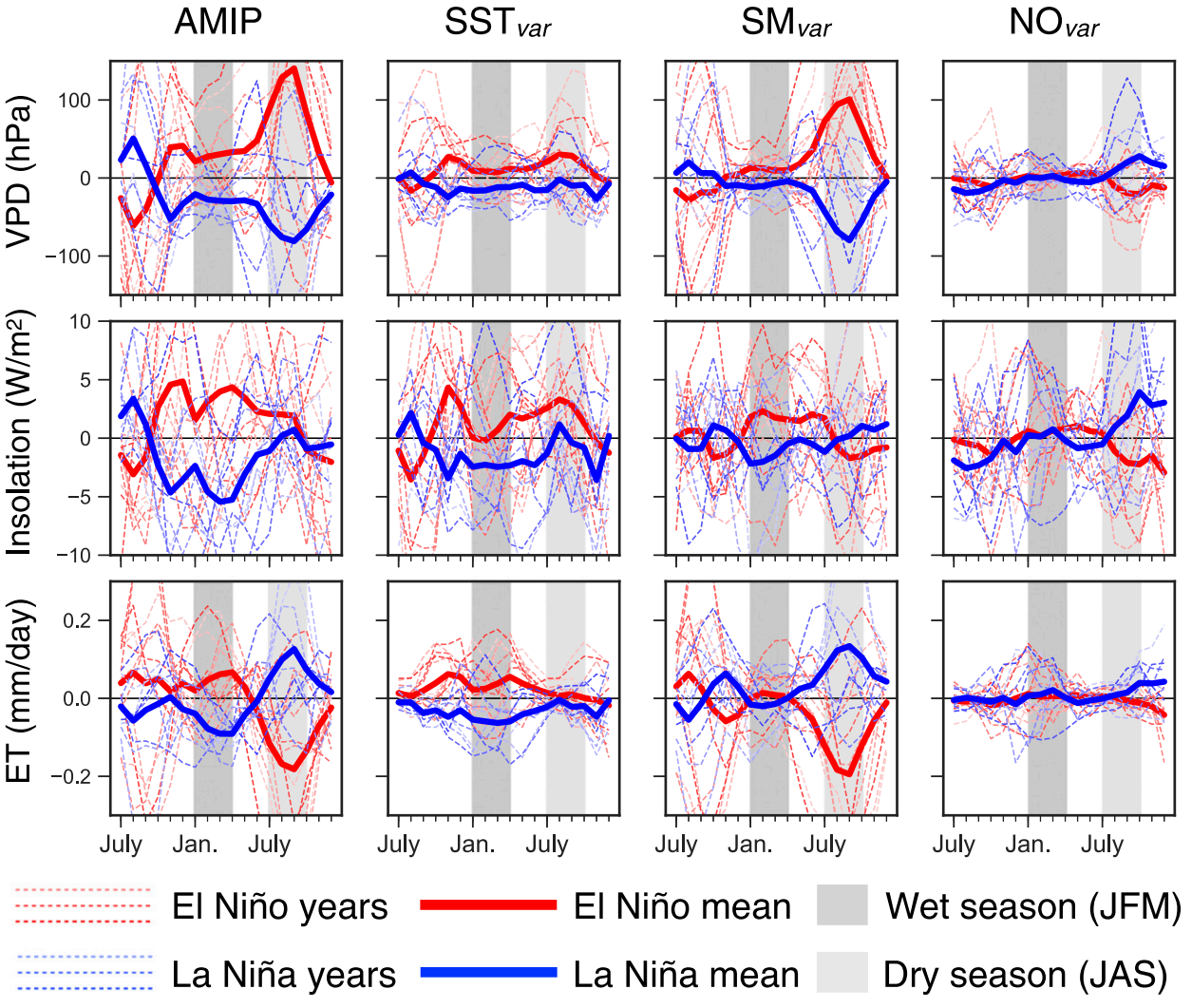

FIG. 8. Temporal evolution of monthly anomalies of biogeophysical variables in the eastern Amazon in the (left to right) AMIP, SST_{var}, SM_{var}, and NO_{var} E3SM simulations. Monthly anomalies of (top) vapor pressure deficit (VPD), (middle) downwelling shortwave radiation (insolation), and (bottom) evapotranspiration (ET) were averaged across all grid cells in the Amazon watershed east of 60°W from the July preceding each El Niño (red) and La Niña (blue) year through the following December. Individual years are plotted with dashed lines, with a solid line for the mean of El Niño and La Niña years. Gray regions delineate the months in the wet season (January–March) and dry season (July–September). Monthly data were smoothed with a 3-month centered moving average for clarity.

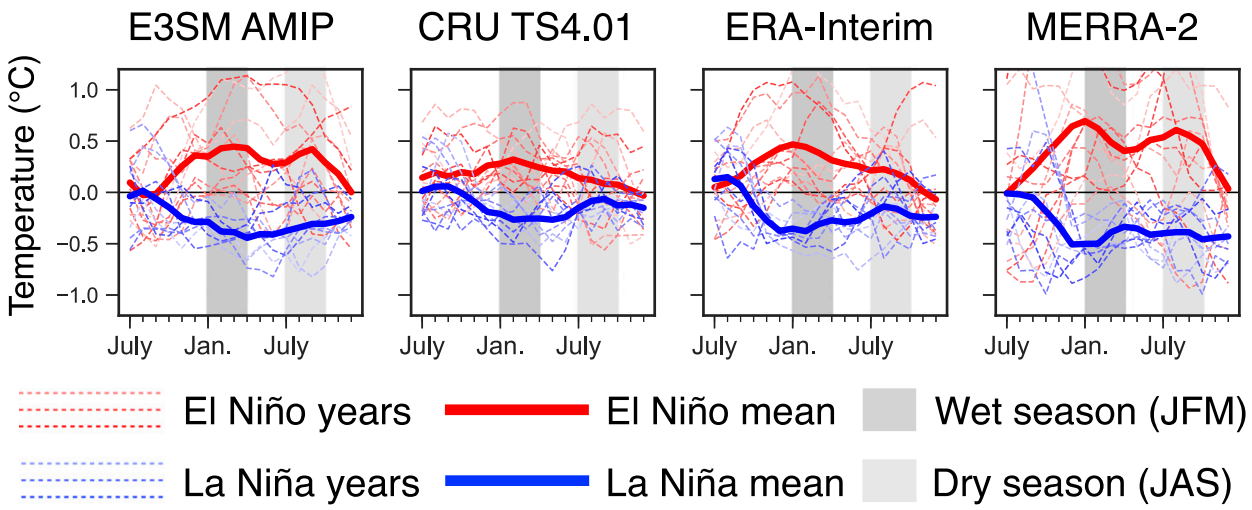

FIG. 9. As in Fig. 7, but for (left to right) the E3SM AMIP simulation and CRU TS4.01, ERA-Interim, and MERRA-2 benchmark datasets.

with a longer time scale (i.e., air temperature lagging SST by 7 or 8 months). The lag-correlation structure of the AMIP simulation was in between those of the SST_{var} and SM_{var} simulations.

For the first few months of lag time, correlations from the AMIP simulation resembled those of the SST_{var} simulation, consistent with initial forcing by SST. But the AMIP structure then attained a higher peak correlation at a longer lag time, and the predictability was prolonged consistent with support from the soil moisture interaction revealed by the SM_{var} correlation. The lagged correlations from benchmark datasets peaked somewhat earlier and lower than those from the AMIP simulation (Fig. 10b). This could also be interpreted as an indication of temperature responding too strongly to soil moisture in E3SM. Alternatively, the timing inconsistency could have resulted from a tendency for ESMs to exhibit a delay in the seasonal cycle of precipitation in this region (Joetzjer et al. 2013).

d. ENSO response of the carbon cycle

The ENSO-driven contrast in net ecosystem exchange (NEE; positive flux to atmosphere) across the E3SM experimental simulations showed a similar seasonal partitioning of drivers to that of the temperature contrast (Fig. 11). During the wet season, the AMIP simulation showed a positive contrast throughout the Amazon basin, resulting from positive NEE anomalies (an increased source and/or reduced sink of atmospheric CO_2) during El Niño and negative anomalies during La Niña. This contrast was present, though reduced in strength, in the SST_{var} simulation, and was largely reversed in the SM_{var} simulation. During the dry season, there was a strong regional difference, particularly in the eastern Amazon, in both the AMIP and SM_{var} simulations that was absent in the SST_{var} simulation. This partitioning of drivers was particularly apparent in the east, which we further examined through the time series of NEE and the ecohydrologic drivers of NEE (Fig. 12).

Interannual anomalies in net primary production (NPP) were driven primarily by soil moisture variability rather than direct SST forcing. NPP was suppressed by drier soils under El Niño conditions and enhanced by wetter soils under La Niña conditions throughout the year in both the AMIP and SM_{var} simulations, with a substantially larger contrast in the dry season than in the wet season. During the wet season, direct SST-driven temperature and radiation anomalies of the same sign (Figs. 7 and 8) had opposite effects on NPP, but the influence of temperature was dominant (e.g., higher El Niño temperatures reduced NPP more than it was enhanced by increased sunlight). However, these NPP contrasts were small compared with those caused by soil moisture variability, particularly during the dry season.

Soil moisture variability was also the dominant driver of anomalies in heterotrophic respiration, but not necessarily for NEE. Dry El Niño soils reduced respiration and wet La Niña soils increased it throughout the year, particularly during the dry season. However, the magnitude of these effects relative to NPP led to distinct differences between the wet and dry seasons.

During the wet season, the coupled ENSO-driven contrast in eastern Amazon NEE was 0.16 $gC\,m^{-2}\,day^{-1}$ (Table 2). Soil moisture effects on NPP and respiration were approximately equal, yielding only a small NEE contrast in the SM_{var} simulation. At the same time, respiration anomalies driven by direct SST forcing on temperature had a similar magnitude to the concurrent NPP anomalies

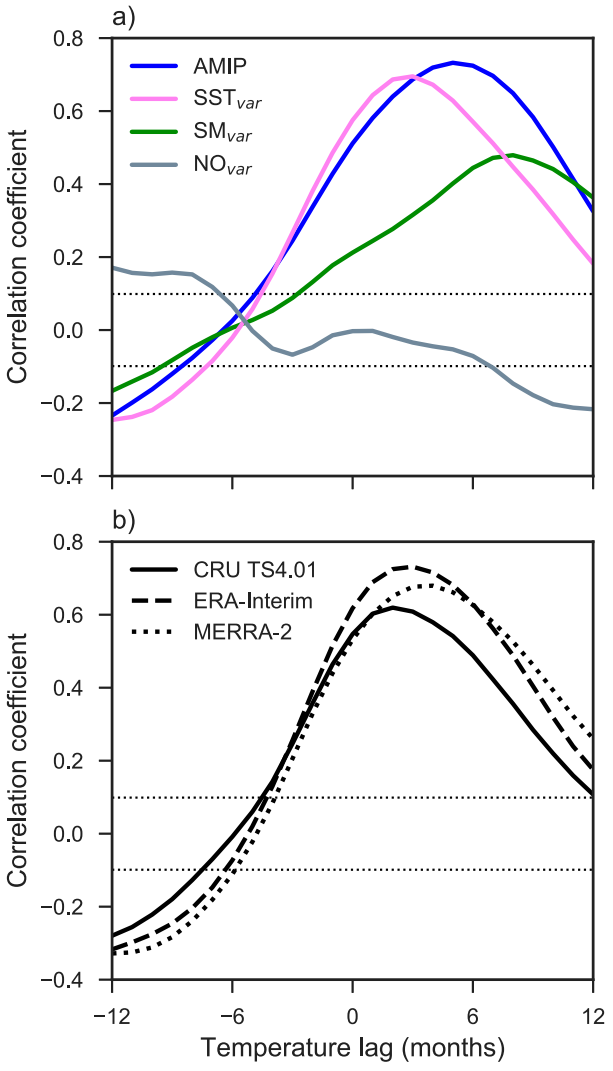

FIG. 10. Temporal structure of Niño-3.4 correlations with lagged surface air temperature in the eastern Amazon for (a) E3SM experiments and (b) benchmark datasets. Monthly temperature anomalies averaged across all grid cells in the Amazon watershed east of 60°W were correlated with the Niño-3.4 index using lead and lag times up to 12 months. Dashed horizontal lines indicate correlation coefficients that are statistically significant at $p \leq 0.05$. Monthly data were smoothed with a 3-month centered moving average for clarity.

but with the opposite sign. As a result, wet-season NEE anomalies were larger than the constituent NPP and respiration anomalies in both the AMIP and SST_{var} simulations. Therefore, despite substantial soil moisture effects on the components of NEE, wet-season C_{SM} was close to zero while C_{SST} was close to 100% (Table 3).

By the dry season, the fully coupled NEE anomalies grew to twice the magnitude of those occurring during the wet season, with an ENSO-driven contrast of 0.32 $gC\,m^{-2}\,day^{-1}$. Soil moisture effects on NPP and respiration were still of the same sign, but the effect on NPP was larger. Therefore, while respiration anomalies dampened the effect of NPP anomalies, there was still a strong NEE contrast in both the SM_{var} and AMIP runs. By this time of year, direct impact of SST forcing on temperature and radiation had weakened, and soil moisture variability was the dominant driver, with a dry season C_{SM} of 85%–91%.

4. Discussion

a. *Land–atmosphere coupling and ENSO*

Our mechanism-denial experiments with E3SM illustrate how soil moisture variability served to intensify and extend the temperature response of the Amazon to forcing from ENSO. SST anomalies, which peaked during December–February, drove changes to atmospheric circulation and meteorology in the Amazon with little or no delay. The direct impact of these changes, absent any soil moisture interaction, was responsible for over four-fifths of the wet-season temperature response to ENSO in the eastern Amazon. Concurrent precipitation anomalies led to a soil moisture memory that persisted into the following dry season, resulting in a delayed temperature response via land–atmosphere coupling. This indirect impact of soil moisture was responsible for two-thirds to four-fifths of the contrast between El Niño and La Niña dry-season temperatures. These results highlight how temperature anomalies set up by ocean–atmosphere climate modes are amplified and extended by land–atmosphere coupling.

Our results also illustrate the importance of soil moisture variability in the ENSO-modulated carbon cycle response of the eastern Amazon. During the wet season, soil moisture impacts on NPP and heterotrophic respiration counteracted each other, leading to a net neutral impact on NEE, while direct SST forcing on each of these fluxes amplified impacts on NEE. This gives direct SST forcing the appearance of driving nearly all of the wet-season ENSO-driven NEE contrast, despite soil moisture impacts on the constituent NPP and respiration anomalies. During the dry season, the carbon cycle response was driven primarily by soil moisture variability, which limited NPP more than heterotrophic respiration. At the same time, the temperature anomalies resulting from land–atmosphere coupling affected NPP with the same sign as the net soil moisture effect, with the NPP response dominating the overall NEE signal. This portion of the temperature anomaly T_{SM} combines with the direct control of soil moisture on NEE, leading to the dominance of C_{SM} during the dry season.

b. *Uncertainties and limitations*

While our experiment demonstrated the importance of land–atmosphere coupling in E3SM, extrapolation to the real Earth system must be tempered by consideration

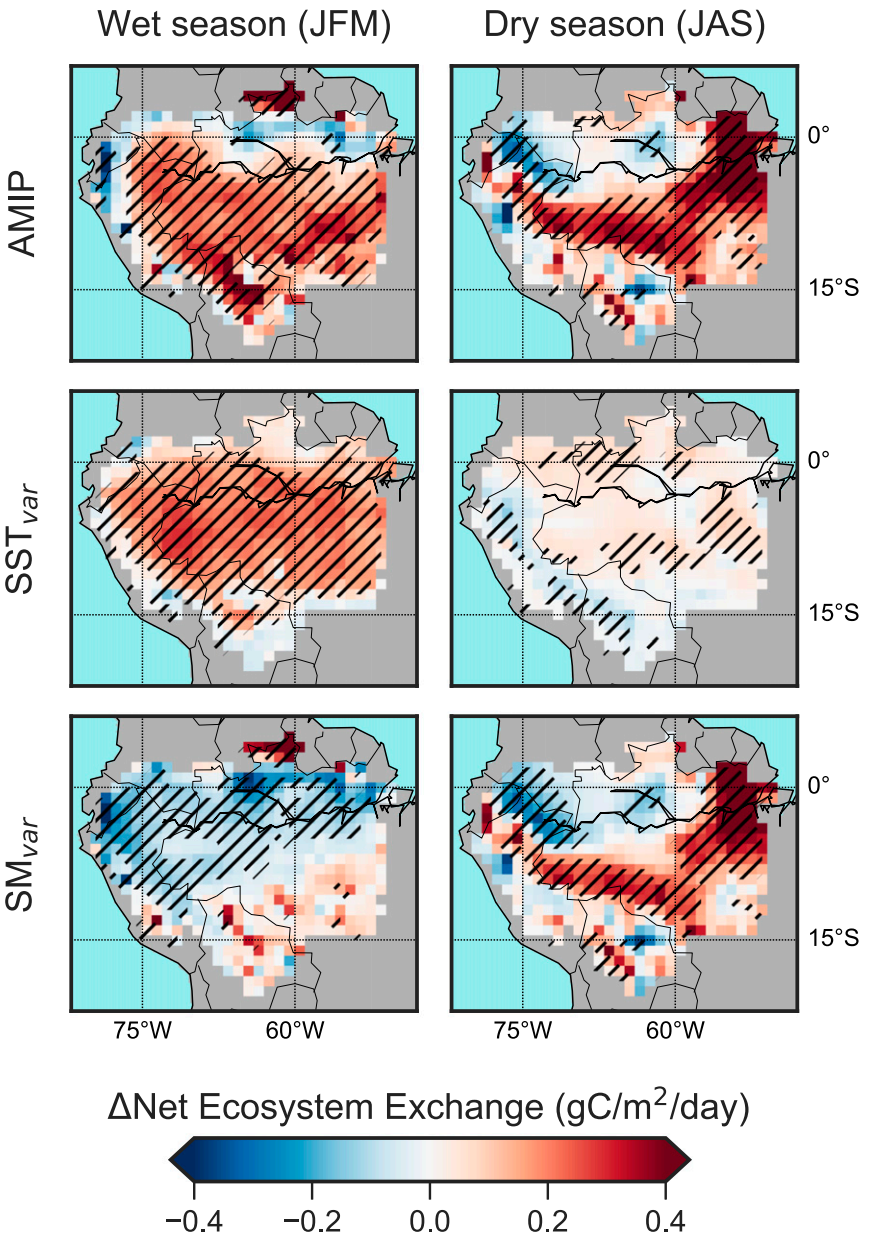

FIG. 11. Difference between NEE (positive flux to atmosphere) anomalies averaged across El Niño and La Niña years during (left) the wet season (January–March) and (right) the dry season (July–September) in the (top) AMIP, (middle) SST_{var}, and (bottom) SM_{var} simulations. Cross-hatching indicates that the difference between El Niño and La Niña means is statistically significant at $p \leq 0.05$.

of the disagreement in the ENSO-driven temperature contrast between observations and reanalyses. The AMIP simulation was able to reproduce the mean temperature within the uncertainty of the benchmark temperature data, but it showed a stronger dry-season contrast than two of the three benchmark datasets. This may have resulted from unrealistically strong land–atmosphere coupling in this model, which would be consistent with previous studies that found land–atmosphere coupling to be too strong in the models on which E3SM is based (Dirmeyer 2006; Zeng et al. 2010; Mei and Wang 2012; Levine et al. 2016).

Land surface temperatures are more sensitive to moisture availability when that becomes the limiting factor for evapotranspiration, which mostly occurs under semiarid conditions (Seneviratne et al. 2010). Therefore, any errors in the model that pushed the Amazon from its generally moist state toward drier

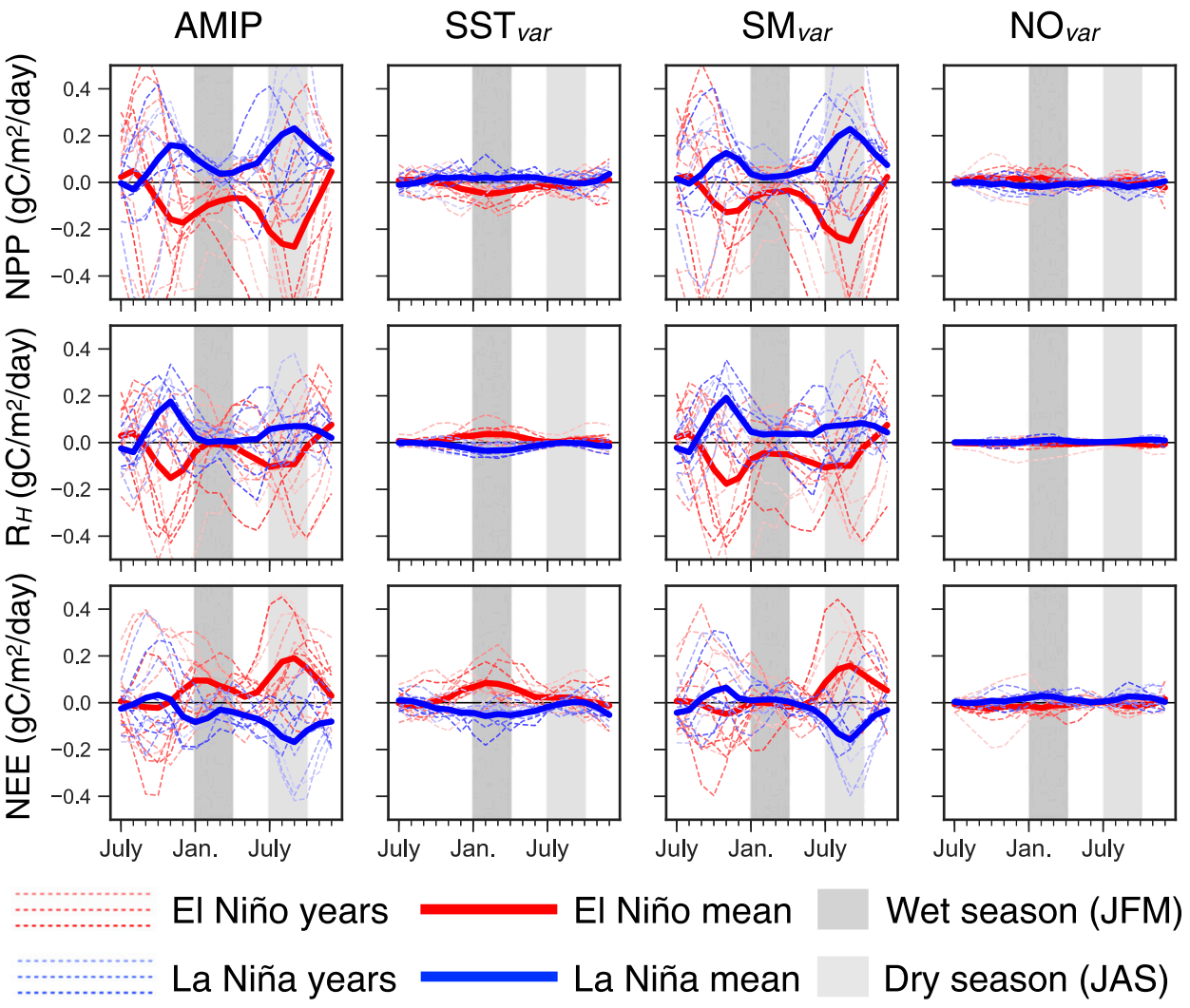

FIG. 12. Temporal evolution of monthly anomalies of ecosystem variables in the eastern Amazon in the (left to right) AMIP, SST_{var}, SM_{var}, and NO_{var} E3SM simulations. Monthly anomalies of (top) net primary production (NPP), (middle) heterotrophic respiration (R_H), and (bottom) net ecosystem exchange (NEE) were averaged across all grid cells in the Amazon watershed east of 60°W from the July preceding each El Niño (red) and La Niña (blue) year through the following December. Individual years are plotted with dashed lines, with a solid line for the mean of El Niño and La Niña years. Gray regions delineate the months in the wet season (January–March) and dry season (July–September). Monthly data were smoothed with a 3-month centered moving average for clarity.

conditions could have biased the land–atmosphere coupling strength. The dry bias in the AMIP simulation is a well-known feature of many ESMs, including the precursors to E3SM (Joetzjer et al. 2013; Yin et al. 2013), and could have caused excessive land–atmosphere coupling that led to an unrealistically large temperature contrast in the dry season. In addition, CLM4.5 does not include any hydraulic redistribution by deep roots (Tang et al. 2015; Y. Wang et al. 2016), which sustains dry-season plant growth and evapotranspiration in the Amazon (Nepstad et al. 1994; Lee et al. 2005; Oliveira et al. 2005). This may also have pushed the model toward drier conditions, by making water inaccessible by plants and unavailable for evapotranspiration.

On the other hand, there is also evidence that supports the possibility that E3SM may have underestimated the response to ENSO. The precipitation bias applied not only to the mean state, but also to the magnitude of interannual variability. Land–atmosphere coupling in the model ensured that errors in wet-season precipitation that yielded errors in subsequent dry-season water storage anomalies would have led to errors in temperature, and potentially NEE as well. Insufficient precipitation variability in the eastern Amazon did not lead to insufficient water storage variability, at least over the

limited time span of the GRACE record. However, in the places where water storage variability was too low, the temperature anomalies resulting from land–atmosphere coupling would also have been too low, which could have caused the simulated response to ENSO to be too weak.

c. *Implications for future research*

Our results suggest that attempts to partition the relative importance of temperature and hydrology in the carbon cycle response to ENSO should consider the interdependence between these variables. In particular, studies that employ offline models that are forced by non-interactive temperature and precipitation (or soil moisture) time series may overestimate the sensitivity of CO_2 fluxes to temperature and underestimate the sensitivity to hydrology (e.g., Piao et al. 2013; Wang et al. 2013). While our experiments could not separate the direct ecosystem carbon response to soil moisture from the effect of soil moisture on temperature, they demonstrated that the largest ENSO-driven carbon cycle anomalies, in the eastern Amazon during the dry season, are spatiotemporally collocated with the strongest land–atmosphere coupling. Future work could use temperature time series from an experiment such as ours to drive an offline model, in order to further constrain how much of C_{SM} is directly due to T_{SM}.

The disagreements between the benchmark temperature datasets highlight the need to reduce uncertainties in observations and reanalyses. CRU TS4.01 is based on station observations, so in sparsely observed regions such as the Amazon spatial interpolation could decrease interannual variability, which could have caused the overall low contrast in this dataset. Reanalysis datasets showed stronger contrasts, but they are constrained at the surface by land surface models that may themselves suffer from the same bias in land–atmosphere coupling strength as E3SM. The ongoing efforts toward improving these data products are important for understanding remote but climatically significant regions such as the Amazon.

5. Conclusions

We performed an experiment with a set of global E3SM simulations to decouple the direct effects of SST variability from the resulting soil moisture variability in the Amazon. We found that soil moisture anomalies served to intensify and prolong the response of the eastern Amazon climate to ENSO. The immediate component of the response to El Niño was driven directly by atmospheric circulation changes that increased temperatures and reduced precipitation during the wet season. Soil moisture anomalies persisted into the dry season, causing a delayed temperature response from land–atmosphere coupling. SST-driven soil moisture anomalies explained two-thirds to four-fifths of the eastern Amazon's dry-season temperature response to ENSO in E3SM. Observational and reanalysis data suggest that E3SM may have overestimated the temperature response to ENSO, perhaps due to a bias in land–atmosphere coupling strength.

The drivers of the carbon cycle response to ENSO in E3SM were similar to those for temperature. In the eastern Amazon, soil moisture did not affect the net carbon cycle response to ENSO during the wet season, but it drove the majority of the dry season response. ENSO had a larger impact on dry-season carbon fluxes than those of the wet season, resulting from soil moisture limitations on ecosystem function combined with land–atmosphere coupling affecting temperature. This indicates the need to consider the interdependent relationship between temperature and the hydrologic cycle when attributing mechanisms to ENSO-driven variability in the tropical terrestrial carbon cycle.

Acknowledgments. We received funding support from the Reducing Uncertainties in Biogeochemical Interactions through Synthesis and Computation Scientific Focus Area (RUBISCO SFA), which is sponsored by the Regional and Global Model Analysis (RGMA) Program in the Climate and Environmental Sciences Division (CESD) of the Office of Biological and Environmental Research (BER) in the U.S. Department of Energy (DOE) Office of Science. This research used resources from Project m2467 of the National Energy Research Scientific Computing Center, a DOE Office of Science User Facility (DE-AC02-05CH11231), and from Project cli106bgc of the Oak Ridge Leadership Computing Facility, which is a DOE Office of Science User Facility (DE-AC05-00OR22725). P.A.L. received funding support from NASA Headquarters under the NASA Earth and Space Science Fellowship Program (NNX16AO38H). J.T.R. and Y.C. received additional funding support from the DOE Office of Science Earth System Modeling Program (DE-SC0006791) and NASA's SMAP and CMS programs. M.S.P. received funding support from the DOE Early Career Program (DE-SC0012152). M.X. and F.M.H. received additional funding support from the Energy Exascale Earth System Model (E3SM) Project and the Next Generation Ecosystem Experiments–Tropics (NGEE-Tropics) Project, sponsored by BER in the DOE Office of Science. Oak Ridge National Laboratory (ORNL) is managed by UT-Battelle, LLC, for the DOE (DE-AC05-00OR22725). GPCP combined precipitation data were provided by the NASA/Goddard Space Flight Center's Laboratory for Atmospheres, which develops and computes the

dataset as a contribution to the GEWEX Global Precipitation Climatology Project, from their website at https://precip.gsfc.nasa.gov. CMAP precipitation data were provided by the NOAA/OAR/ESRL PSD, Boulder, Colorado, USA, from their Web site at https://www.esrl.noaa.gov/psd. GRACE terrestrial water storage data are available at http://grace.jpl.nasa.gov, supported by the NASA MEaSUREs Program. CRU TS data were obtained from the University of East Anglia through their website at https://crudata.uea.ac.uk. ERA-Interim data were obtained from the European Centre for Medium-Range Weather Forecasts through their website at http://apps.ecmwf.int/datasets. MERRA-2 data were obtained from the Goddard Earth Sciences Data and Information Services Center through their website at https://disc.sci.gsfc.nasa.gov. E3SM output from this experiment is archived on the National Energy Research Scientific Computing Center's High Performance Storage System and is available for download at http://portal.nersc.gov/archive/home/p/plevine/www/data_archive/e3sm_enso.

REFERENCES

Bacastow, R. B., 1976: Modulation of atmospheric carbon dioxide by the Southern Oscillation. *Nature*, **261**, 116–118, https://doi.org/10.1038/261116a0.

Banzon, V., T. M. Smith, T. M. Chin, C. Liu, and W. Hankins, 2016: A long-term record of blended satellite and in situ sea-surface temperature for climate monitoring, modeling and environmental studies. *Earth Syst. Sci. Data*, **8**, 165–176, https://doi.org/10.5194/essd-8-165-2016.

Bowman, K. W., and Coauthors, 2017: Global and Brazilian carbon response to El Niño Modoki 2011–2010. *Earth Space Sci.*, **4**, 637–660, https://doi.org/10.1002/2016EA000204.

Chen, Y., and Coauthors, 2011: Forecasting fire season severity in South America using sea surface temperature anomalies. *Science*, **334**, 787–791, https://doi.org/10.1126/science.1209472.

——, I. Velicogna, J. S. Famiglietti, and J. T. Randerson, 2013: Satellite observations of terrestrial water storage provide early warning information about drought and fire season severity in the Amazon. *J. Geophys. Res. Biogeosci.*, **118**, 495–504, https://doi.org/10.1002/jgrg.20046.

——, D. C. Morton, N. Andela, G. R. van der Werf, L. Giglio, and J. T. Randerson, 2017: A pan-tropical cascade of fire driven by El Niño/Southern Oscillation. *Nat. Climate Change*, **7**, 906–911, https://doi.org/10.1038/s41558-017-0014-8.

Cox, P. M., D. Pearson, B. B. Booth, P. Friedlingstein, C. Huntingford, C. D. Jones, and C. M. Luke, 2013: Sensitivity of tropical carbon to climate change constrained by carbon dioxide variability. *Nature*, **494**, 341–344, https://doi.org/10.1038/nature11882.

Dee, D. P., and Coauthors, 2011: The ERA-Interim reanalysis: Configuration and performance of the data assimilation system. *Quart. J. Roy. Meteor. Soc.*, **137**, 553–597, https://doi.org/10.1002/qj.828.

de Linage, C., H. Kim, J. S. Famiglietti, and J.-Y. Yu, 2013: Impact of Pacific and Atlantic sea surface temperatures on interannual and decadal variations of GRACE land water storage in tropical South America. *J. Geophys. Res. Atmos.*, **118**, 10 811–10 829, https://doi.org/10.1002/jgrd.50820.

Dennis, J. M., and Coauthors, 2012: CAM-SE: A scalable spectral element dynamical core for the Community Atmosphere Model. *Int. J. High Perform. Comput. Appl.*, **26**, 74–89, https://doi.org/10.1177/1094342011428142.

Dirmeyer, P. A., 2006: The hydrologic feedback pathway for land–climate coupling. *J. Hydrometeor.*, **7**, 857–867, https://doi.org/10.1175/JHM526.1.

Foley, J. A., A. Botta, M. T. Coe, and M. H. Costa, 2002: El Niño–Southern Oscillation and the climate, ecosystems and rivers of Amazonia. *Global Biogeochem. Cycles*, **16**, 1132, https://doi.org/10.1029/2002GB001872.

Fu, R., R. E. Dickinson, M. Chen, and H. Wang, 2001: How do tropical sea surface temperatures influence the seasonal distribution of precipitation in the equatorial Amazon? *J. Climate*, **14**, 4003–4026, https://doi.org/10.1175/1520-0442(2001)014<4003:HDTSST>2.0.CO;2.

Gates, W. L., and Coauthors, 1999: An overview of the results of the Atmospheric Model Intercomparison Project (AMIP I). *Bull. Amer. Meteor. Soc.*, **80**, 29–55, https://doi.org/10.1175/1520-0477(1999)080<0029:AOOTRO>2.0.CO;2.

Gelaro, R., and Coauthors, 2017: The Modern-Era Retrospective Analysis for Research and Applications, version 2 (MERRA-2). *J. Climate*, **30**, 5419–5454, https://doi.org/10.1175/JCLI-D-16-0758.1.

Harris, I., P. Jones, T. Osborn, and D. Lister, 2014: Updated high-resolution grids of monthly climatic observations—The CRU TS3.10 dataset. *Int. J. Climatol.*, **34**, 623–642, https://doi.org/10.1002/joc.3711.

Hilker, T., and Coauthors, 2014: Vegetation dynamics and rainfall sensitivity of the Amazon. *Proc. Natl. Acad. Sci. USA*, **111**, 16 041–16 046, https://doi.org/10.1073/pnas.1404870111.

Huffman, G. J., R. F. Adler, D. T. Bolvin, and G. Gu, 2009: Improving the global precipitation record: GPCP version 2.1. *Geophys. Res. Lett.*, **36**, L17808, https://doi.org/10.1029/2009GL040000.

Humphrey, V., J. Zscheischler, P. Ciais, L. Gudmundsson, S. Sitch, and S. I. Seneviratne, 2018: Sensitivity of atmospheric CO_2 growth rate to observed changes in terrestrial water storage. *Nature*, **560**, 628–631, https://doi.org/10.1038/s41586-018-0424-4.

Jiménez-Muñoz, J. C., C. Mattar, J. Barichivich, A. Santamaría-Artigas, K. Takahashi, Y. Malhi, J. Sobrino, and G. van der Schrier, 2016: Record-breaking warming and extreme drought in the Amazon rainforest during the course of El Niño 2015–2016. *Sci. Rep.*, **6**, 33130, https://doi.org/10.1038/srep33130.

Joetzjer, E., H. Douville, C. Delire, and P. Ciais, 2013: Present-day and future Amazonian precipitation in global climate models: CMIP5 versus CMIP3. *Climate Dyn.*, **41**, 2921–2936, https://doi.org/10.1007/s00382-012-1644-1.

Jones, C. D., M. Collins, P. M. Cox, and S. A. Spall, 2001: The carbon cycle response to ENSO: A coupled climate–carbon cycle model study. *J. Climate*, **14**, 4113–4129, https://doi.org/10.1175/1520-0442(2001)014<4113:TCCRTE>2.0.CO;2.

Keeling, C. D., and R. Revelle, 1985: Effects of El Niño/Southern Oscillation on the atmospheric content of carbon dioxide. *Meteoritics*, **20**, 437–450.

Keppel-Aleks, G., and Coauthors, 2014: Separating the influence of temperature, drought, and fire on interannual variability in atmospheric CO_2. *Global Biogeochem. Cycles*, **28**, 1295–1310, https://doi.org/10.1002/2014GB004890.

Lee, J.-E., R. S. Oliveira, T. E. Dawson, and I. Fung, 2005: Root functioning modifies seasonal climate. *Proc. Natl. Acad. Sci. USA*, **102**, 17 576–17 581, https://doi.org/10.1073/pnas.0508785102.

——, B. R. Lintner, C. K. Boyce, and P. J. Lawrence, 2011: Land use change exacerbates tropical South American drought by

sea surface temperature variability. *Geophys. Res. Lett.*, **38**, L19706, https://doi.org/10.1029/2011GL049066.

Levine, P. A., J. T. Randerson, S. C. Swenson, and D. M. Lawrence, 2016: Evaluating the strength of the land–atmosphere moisture feedback in Earth system models using satellite observations. *Hydrol. Earth Syst. Sci.*, **20**, 4837–4856, https://doi.org/10.5194/hess-20-4837-2016.

Liu, J., and Coauthors, 2017: Contrasting carbon cycle responses of the tropical continents to the 2015–2016 El Niño. *Science*, **358**, https://doi.org/10.1126/science.aam5690.

Llovel, W., and Coauthors, 2011: Terrestrial waters and sea level variations on interannual time scale. *Global Planet. Change*, **75**, 76–82, https://doi.org/10.1016/j.gloplacha.2010.10.008.

Ma, H.-Y., C. R. Mechoso, Y. Xue, H. Xiao, C.-M. Wu, J.-L. Li, and F. De Sales, 2011: Impact of land surface processes on the South American warm season climate. *Climate Dyn.*, **37**, 187–203, https://doi.org/10.1007/s00382-010-0813-3.

Marengo, J. A., 1992: Interannual variability of surface climate in the Amazon Basin. *Int. J. Climatol.*, **12**, 853–863, https://doi.org/10.1002/joc.3370120808.

Mei, R., and G. Wang, 2012: Summer land–atmosphere coupling strength in the United States: Comparison among observations, reanalysis data, and numerical models. *J. Hydrometeor.*, **13**, 1010–1022, https://doi.org/10.1175/JHM-D-11-075.1.

Miguez-Macho, G., and Y. Fan, 2012: The role of groundwater in the amazon water cycle: 2. Influence on seasonal soil moisture and evapotranspiration. *J. Geophys. Res.*, **117**, D15114, https://doi.org/10.1029/2012JD017540.

Neale, R. B., and Coauthors, 2012: Description of the NCAR Community Atmosphere Model (CAM 5.0). NCAR Tech. Note NCAR/TN-486+STR, 274 pp., www.cesm.ucar.edu/models/cesm1.0/cam/docs/description/cam5_desc.pdf.

Negrón Juárez, R. I., M. G. Hodnett, R. Fu, M. L. Goulden, and C. von Randow, 2007: Control of dry season evapotranspiration over the Amazonian forest as inferred from observations at a southern Amazon forest site. *J. Climate*, **20**, 2827–2839, https://doi.org/10.1175/JCLI4184.1.

Nepstad, D. C., and Coauthors, 1994: The role of deep roots in the hydrological and carbon cycles of Amazonian forests and pastures. *Nature*, **372**, 666–669, https://doi.org/10.1038/372666a0.

Oleson, K. W., and Coauthors, 2013: Technical description of version 4.5 of the Community Land Model (CLM). NCAR Tech. Rep. NCAR/TN-503+STR, 420 pp., https://doi.org/10.5065/D6RR1W7M.

Oliveira, R. S., T. E. Dawson, S. S. O. Burgess, and D. C. Nepstad, 2005: Hydraulic redistribution in three Amazonian trees. *Oecologia*, **145**, 354–363, https://doi.org/10.1007/s00442-005-0108-2.

Orth, R., and S. I. Seneviratne, 2017: Variability of soil moisture and sea surface temperatures similarly important for warm-season land climate in the Community Earth System Model. *J. Climate*, **30**, 2141–2162, https://doi.org/10.1175/JCLI-D-15-0567.1.

Piao, S., and Coauthors, 2013: Evaluation of terrestrial carbon cycle models for their response to climate variability and to CO_2 trends. *Global Change Biol.*, **19**, 2117–2132, https://doi.org/10.1111/gcb.12187.

Qian, H., R. Joseph, and N. Zeng, 2008: Response of the terrestrial carbon cycle to the El Niño–Southern Oscillation. *Tellus*, **60B**, 537–550, https://doi.org/10.1111/j.1600-0889.2008.00360.x.

Reager, J. T., A. S. Gardner, J. S. Famiglietti, D. N. Wiese, A. Eicker, and M.-H. Lo, 2016: A decade of sea level rise slowed by climate-driven hydrology. *Science*, **351**, 699–703, https://doi.org/10.1126/science.aad8386.

Seneviratne, S. I., T. Corti, E. L. Davin, M. Hirschi, E. B. Jaeger, I. Lehner, B. Orlowsky, and A. J. Teuling, 2010: Investigating soil moisture–climate interactions in a changing climate: A review. *Earth Sci. Rev.*, **99**, 125–161, https://doi.org/10.1016/j.earscirev.2010.02.004.

——, and Coauthors, 2013: Impact of soil moisture–climate feedbacks on CMIP5 projections: First results from the GLACE-CMIP5 experiment. *Geophys. Res. Lett.*, **40**, 5212–5217, https://doi.org/10.1002/grl.50956.

Spennemann, P. C., and A. C. Saulo, 2015: An estimation of the land–atmosphere coupling strength in South America using the Global Land Data Assimilation System. *Int. J. Climatol.*, **35**, 4151–4166, https://doi.org/10.1002/joc.4274.

Sun, S., and G. Wang, 2013: Climate variability attributable to terrestrial and oceanic forcing in the NCAR CAM3-CLM3 models. *Climate Dyn.*, **42**, 2067–2078, https://doi.org/10.1007/s00382-013-1913-7.

Swann, A. L. S., and C. D. Koven, 2017: A direct estimate of the seasonal cycle of evapotranspiration over the Amazon basin. *J. Hydrometeor.*, **18**, 2173–2185, https://doi.org/10.1175/JHM-D-17-0004.1.

Tang, J., W. J. Riley, and J. Niu, 2015: Incorporating root hydraulic redistribution in CLM4.5: Effects on predicted site and global evapotranspiration, soil moisture, and water storage. *J. Adv. Model. Earth Syst.*, **7**, 1828–1848, https://doi.org/10.1002/2015MS000484.

Taylor, K. E., 2001: Summarizing multiple aspects of model performance in a single diagram. *J. Geophys. Res.*, **106**, 7183–7192, https://doi.org/10.1029/2000JD900719.

Terai, C. R., P. M. Caldwell, S. A. Klein, Q. Tang, and M. L. Branstetter, 2018: The atmospheric hydrologic cycle in the ACME v0.3 model. *Climate Dyn.*, **50**, 3251–3279, https://doi.org/10.1007/s00382-017-3803-x.

Trenberth, K. E., J. M. Caron, D. P. Stepaniak, and S. Worley, 2002: Evolution of El Niño–Southern Oscillation and global atmospheric surface temperatures. *J. Geophys. Res.*, **107**, 4065, https://doi.org/10.1029/2000JD000298.

Tyrrell, N. L., D. Dommenget, C. Frauen, S. Wales, and M. Rezny, 2015: The influence of global sea surface temperature variability on the large-scale land surface temperature. *Climate Dyn.*, **44**, 2159–2176, https://doi.org/10.1007/s00382-014-2332-0.

Wang, J., N. Zeng, and M. Wang, 2016: Interannual variability of the atmospheric CO_2 growth rate: Roles of precipitation and temperature. *Biogeosciences*, **13**, 2339–2352, https://doi.org/10.5194/bg-13-2339-2016.

Wang, W., and Coauthors, 2013: Variations in atmospheric CO_2 growth rates coupled with tropical temperature. *Proc. Natl. Acad. Sci. USA*, **110**, 13 061–13 066, https://doi.org/10.1073/pnas.1219683110.

Wang, X., and Coauthors, 2014: A two-fold increase of carbon cycle sensitivity to tropical temperature variations. *Nature*, **506**, 212–215, https://doi.org/10.1038/nature12915.

Wang, Y., Z. Xie, and B. Jia, 2016b: Incorporation of a dynamic root distribution into CLM4.5: Evaluation of carbon and water fluxes over the Amazon. *Adv. Atmos. Sci.*, **33**, 1047–1060, https://doi.org/10.1007/s00376-016-5226-8.

Watkins, M. M., D. N. Wiese, D.-N. Yuan, C. Boening, and F. W. Landerer, 2015: Improved methods for observing Earth's time variable mass distribution with GRACE using spherical cap mascons. *J. Geophys. Res. Solid Earth*, **120**, 2648–2671, https://doi.org/10.1002/2014JB011547.

Wiese, D. N., D.-N. Yuan, C. Boening, F. W. Landerer, and M. M. Watkins, 2015: JPL GRACE Mascon Ocean, Ice, and Hydrology

Equivalent Water Height JPL RL05M.1. Ver. 1. PO.DAAC, accessed 29 September 2018, https://doi.org/10.5067/TEMSC-OCL05.

Xie, P., and P. A. Arkin, 1997: Global precipitation: A 17-year monthly analysis based on gauge observations, satellite estimates, and numerical model outputs. *Bull. Amer. Meteor. Soc.*, **78**, 2539–2558, https://doi.org/10.1175/1520-0477(1997)078<2539:GPAYMA>2.0.CO;2.

Yin, L., R. Fu, E. Shevliakova, and R. E. Dickinson, 2013: How well can CMIP5 simulate precipitation and its controlling processes over tropical South America? *Climate Dyn.*, **41**, 3127–3143, https://doi.org/10.1007/s00382-012-1582-y.

Zeng, N., A. Mariotti, and P. Wetzel, 2005: Terrestrial mechanisms of interannual CO_2 variability. *Global Biogeochem. Cycles*, **19**, GB1016, https://doi.org/10.1029/2004GB002273.

Zeng, X., M. Barlage, C. Castro, and K. Fling, 2010: Comparison of land–precipitation coupling strength using observations and models. *J. Hydrometeor.*, **11**, 979–994, https://doi.org/10.1175/2010JHM1226.1.